Low-phosphorus concentrations and important ferric hydroxide scavenging in Archean seawater

Eric Siciliano Rego, Vincent Busigny, Stefan V Lalonde, Camille Rossignol, Marly Babinski, Pascal Philippot

PNAS Nexus, 2023, 2, 1–7
https://doi.org/10.1093/pnasnexus/pgad025
Advance access publication 8 February 2023
Research Report

Low-phosphorus concentrations and important ferric hydroxide scavenging in Archean seawater

Eric Siciliano Rego[a,b,*1], Vincent Busigny[c], Stefan V. Lalonde[d], Camille Rossignol[e], Marly Babinski[a] and Pascal Philippot[b,f]

[a]Instituto de Geociências, Departamento de Mineralogia e Geotectônica, Universidade de São Paulo, Rua do Lago 562, Cidade Universitária, São Paulo, 05508-080, Brasil
[b]Géosciences Montpellier, Pl. Eugène Bataillon, Campus Triolet, Université de Montpellier, CNRS, Université des Antilles, 34095, Montpellier, France
[c]Université Paris Cité, Institut de physique du globe de Paris, CNRS, 1 Rue Jussieu, 75238 Paris cedex 05, France
[d]CNRS-UMR6538 Laboratoire Geo-Ocean, Institut Universitaire Européen de la Mer, Université de Bretagne Occidentale, Technopôle Brest-Iroise, Rue Dumont d'Urville, 29280, Plouzané, France
[e]Dipartimento di Scienze Chimiche e Geologiche, Università degli Studi di Cagliari, Str. interna Policlinico Universitario, 09042 Monserrato, Cagliari, Italia.
[f]Departamento de Geofísica, Instituto de Astronomia, Geofísica e Ciências Atmosféricas, Universidade de São Paulo, Rua do Matão 1226, Cidade Universitária, São Paulo, 05508-090, Brasil
*To whom correspondence should be addressed: Email: ersiciliano@usp.br
[1]Present address: Origins Laboratory, Department of Geophysical Sciences and Enrico Fermi Institute, The University of Chicago, Chicago, IL 60637, USA.
Edited By: Yannis Yortsos

Abstract

The availability of nutrients in seawater, such as dissolved phosphorus (P), is thought to have regulated the evolution and activity of microbial life in Earth's early oceans. Marine concentrations of bioavailable phosphorus spanning the Archean Eon remain a topic of debate, with variable estimates indicating either low (0.04 to 0.13 μM P) or high (10 to 100 μM P) dissolved P in seawater. The large uncertainty on these estimates reflects in part a lack of clear proxy signals recorded in sedimentary rocks. Contrary to some recent views, we show here that iron formations (IFs) are reliable recorders of past phosphorus concentrations and preserved a primary seawater signature. Using measured P and iron (Fe) contents in Neoarchean IF from Carajás (Brazil), we demonstrate for the first time a clear partitioning coefficient relationship in the P-Fe systematics of this IF, which, in combination with experimental and Archean literature data, permits us to constrain Archean seawater to a mean value of 0.063 ± 0.05 μM dissolved phosphorus. Our data set suggests that low-phosphorus conditions prevailed throughout the first half of Earth's history, likely as the result of limited continental emergence and marine P removal by iron oxyhydroxide precipitation, supporting prior suggestions that changes in ancient marine P availability at the end of the Archean modulated marine productivity, and ultimately, the redox state of Earth's early oceans and atmosphere.

Classification: Physical Sciences, Earth, Atmospheric and Planetary Sciences

Keywords: phosphorus, Archean, iron formations

Significance Statement

The evolution of life in Earth's oceans is thought to have been dependent on nutrient availability, such as dissolved phosphorus (P) in seawater. Quantitatively assessing P concentrations in ancient oceans, however, is challenging and a highly debated topic. Here, we report a correlation between P and Fe contents measured in 2.74 billion-year-old iron formations and carbonates showing the same characteristics as those recorded in modern sediments. We further show that, similarly to present-day environments, Fe-oxide adsorption was a major exit flux of phosphorus from seawater. Our results, combined with available experimental data from the literature, argue for strongly limited P contents on early Earth.

Introduction

Phosphorus (P) is an essential nutrient for all living organisms on Earth and its availability has been crucial for the development and proliferation of life on geological time scales (1). In the oceans, P availability has a significant control on biological productivity, and its concentration throughout Earth's history likely modulated the redox state of the ocean and atmosphere (2–4). Quantitatively assessing past oceanic P levels based on the geological record has been a major challenge, largely due to a lack of robust mineralogical or geochemical proxies that provide unambiguous records of water column P concentrations. Despite the challenge posed by the limited sedimentary record, understanding the ancient marine P cycle is of paramount importance for understanding biological and geochemical evolution through time (5, 6).

Competing Interest: The authors declare no competing interest.
Received: July 8, 2022. **Revised:** November 26, 2022. **Accepted:** January 19, 2023

Reconstructions of dissolved P concentrations in Precambrian oceans are highly debated and rely to a large extent on iron (Fe) and P contents measured in iron-rich chemical sediments, which are interpreted to reflect seawater conditions at their time of formation (2, 5, 7). Previous works support contrasting views of either low dissolved P concentrations in Archean seawater (<1 μM) compared with average modern values (~2.3 μM) (2, 7), or a significantly higher P content in seawater, particularly prior to 2.45 Ga, with proposed concentrations ranging from 5 to 50 times higher than modern values (~10 to 100 μM) (8, 9).

Phosphorus concentrations in ancient seawater can be estimated using the phosphorus to iron ratio (P/Fe) in well-preserved Fe-rich chemical sedimentary rocks (2, 5, 7, 10). This relies on the premise that iron oxide P/Fe ratios scale linearly as a function of ambient dissolved phosphate (PO_4^{3-}) concentrations according to a predictable distribution coefficient model, as observed to occur in modern hydrothermal plumes (11). In this approach, dissolved phosphate concentration (P_D) in a given solution is equal to the P/Fe ratios in ferric oxyhydroxide precipitates divided by a specific distribution coefficient (K_D) representative of the fluid's composition, such that $[P_D] = (1/K_D) \times P/Fe$ (2). Given that K_D values will change in relation to the fluid's composition, as shown by the enrichment and/or depletion of Si and divalent cations (Ca^{2+}, Mg^{2+}) inhibiting and/or facilitating P adsorption, experimental studies have proposed distribution coefficients representative of Archean and Proterozoic seawater (7, 10), thus allowing new estimates of dissolved P in ancient ocean to be determined.

However, despite a clear correlation between P and Fe in modern sediments (11, 12), no such evidence has ever been reported in samples from the Precambrian rock record. In contrast, a lack of correlation was observed in ~2.45 Ga old iron formations (IFs) from Australia and South Africa, suggesting that these rocks did not capture past oceanic conditions (8). It remains to be seen whether other IF deposits may record P-Fe systematics indicative of P uptake behavior conforming to the distribution coefficient model and thus may be useful for constraining the paleomarine P reservoir. Here, we use P and Fe contents from Archean iron-rich chemical sediments to investigate the potential of IFs as recorders of past P contents in seawater and to estimate dissolved P concentrations in seawater prior to the great oxidation event (GOE). Our work is based on Neoarchean (~2.74 Ga) sedimentary rocks from Carajás, Brazil, along with previously published P/Fe ratios from Archean IFs, modern environmental data, and laboratory experiments. The sedimentary succession studied (see Figs. S1–S3) includes IFs intercalated with several Fe-rich and Fe-poor carbonate intervals, therefore representing an opportunity for evaluating P levels in the ocean independently of these lithological variations. Here, we demonstrate a clear example from the Archean sedimentary record of the positive P-Fe scaling relationship expected from P adsorption to Fe oxide, confirming the predominance of Fe oxide as a P sink in these samples and firmly validating the distribution coefficient approach for reconstruction of the ancient marine P reservoir. Collectively, the results provide key insights into past nutrient availability, which likely influenced the dynamics of oxygen production and accumulation in Earth's Precambrian oceans and atmosphere.

Results and discussion

Identifying an Archean Fe-P trap

The weight percent (wt.%) variations of P_2O_5 and total Fe (Fe_2O_3) in the studied IF samples range from 0.076 to 0.1 wt.% and 37.7 to 63.1 wt.%, respectively, while Fe-carbonates (Fe-rich and Fe-poor) have P_2O_5 and Fe_2O_3 contents varying between 0.039 and 0.079 wt.% and between 16.9 and 45.8 wt.%, respectively (Table S1). A well-defined positive correlation is observed between the concentrations of P_2O_5 and Fe_2O_3 measured in the different chemical sedimentary lithologies from the Carajás Formation (Fig. 1A). In contrast, P_2O_5 shows rough inverse relationships with CaO, MgO, and MnO contents (Fig. S4), indicating that iron is the main ligand of phosphorus and that carbonate-rich samples contain less phosphorus. Aluminum is a very minor component in Carajas samples ($Al_2O_3 < 0.1$ wt%) and shows no correlation with phosphorus content (Fig. S4). Moreover, when compared with whole-rock IF literature data filtered for low detritus (<0.3 wt.% Al), our samples are within the range of values measured for other Archean samples (3.8 to 2.6 Ga, Fig. 1B), although less scattered. Our results show a similar trend to the one measured in modern hydrothermal systems (e.g. positive correlation between P_2O_5 and Fe_2O_3) but with a different slope. The modern correlation is interpreted as reflecting the adsorption of dissolved bioavailable phosphate (PO_4^{3-}) onto Fe-oxide precipitates (11–13). Previous studies relied on this observational model to propose an active P-removal from seawater by Fe-oxide precipitation in the Archean ocean (Fe-P trap; 2, 7). Potential phosphite species that may have been generated during sedimentary diagenesis (e.g. 14) are ignored, as these are negligible in the modern marine P budget, unreported at present for rocks deposited after 3.5 Ga (15) and counter indicated in our sample set by the consistent relationship between P and Fe.

The trend defined by the Carajás samples consisting of different rock types (carbonates and IFs) further supports the interpretation that Fe-oxides were likely responsible for P removal from seawater during the Archean, as observed in modern environments (Fig. 1). This, in turn, indicates that ferric oxyhydroxides, and not simply ferrous hydroxides, were primary mineral phases in IFs (e.g. 24). More importantly, our data demonstrate empirically for the first time that IFs may indeed show P-Fe systematics consistent with aqueous adsorptive and co-precipitative partitioning according to the distribution coefficient model. This evidence confirms that a Fe-P trap mechanism was in fact operating, certainly for the Carajás IF (2.74 Ga), and probably for others deposited between 3.8 and 2.6 Ga. Whether this mechanism limited past ocean P availability (e.g. dissolved P concentrations) is still an ongoing question (8) and requires further assessment. Nonetheless, given the correlation between P and Fe for the Carajás samples ($R^2 = 0.97$), we can estimate the concentration of dissolved P in seawater using the slope of the linear regression (~0.0013) combined with previous published distribution coefficient ($[K_D]$) values (Tables 1 and S2).

Archean P vs. Fe trend—preservation vs. alteration

The Archean literature data set broadly overlaps with the newly analyzed Carajás samples. However, literature values display larger scattering in P-Fe space ($R^2 = 0.34$), which contrasts with well-correlated Carajás values (e.g. $R^2 = 0.97$; Fig. 2). Such differences could be related to rock preservation effects. For instance, a loss of Fe and/or P during diagenetic and metamorphic reactions would be expected to produce some variability, hence scattering, in the primary composition of the sediments. These conditions are observed in the ancient rock record, where Fe can be leached by metasomatic fluids (25), and also in modern environments analogous of Archean settings, where the reduction and dissolution of ferric oxyhydroxides release previously adsorbed phosphate to

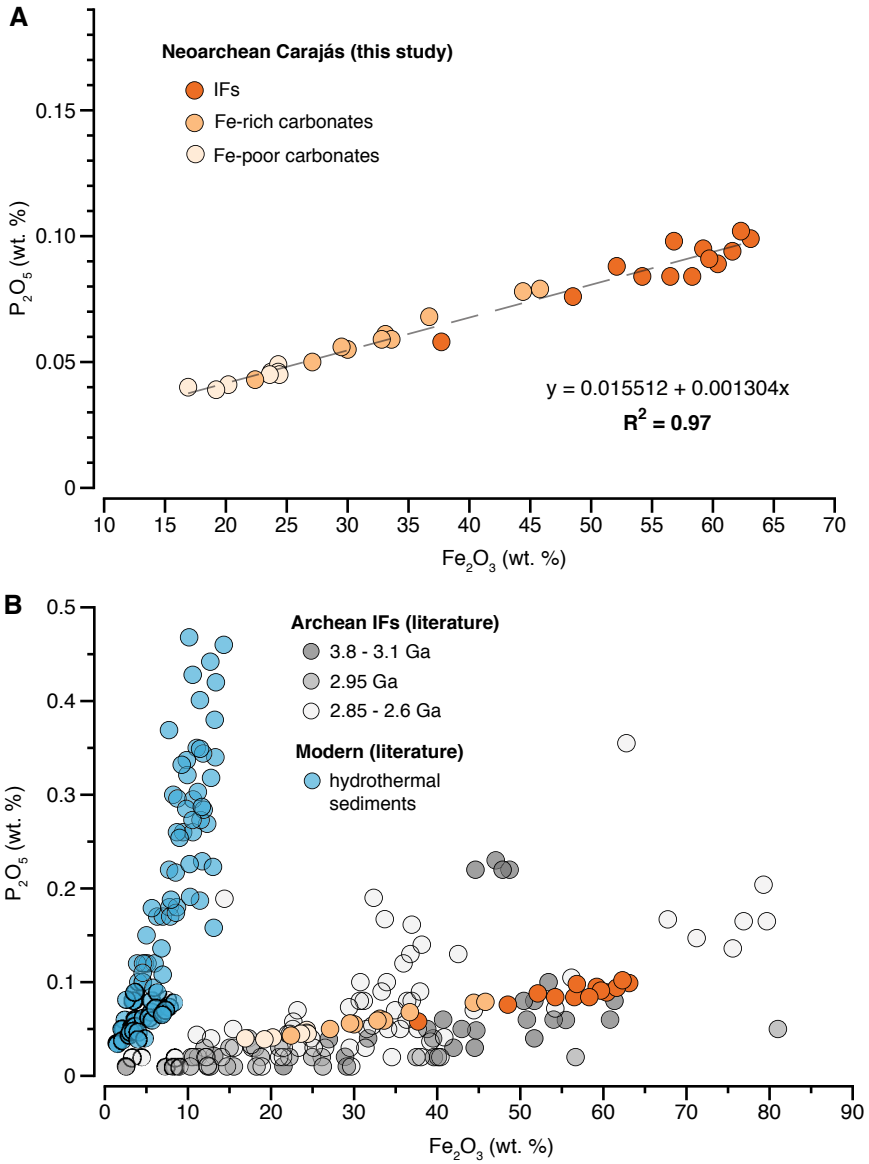

Fig. 1. Variations of bulk Fe_2O_3 and P_2O_5 measured in (A) Neoarchean (~2.74 Ga old) iron formations, Fe-rich and Fe-poor carbonates from Carajás Brazil, and compared in (B) with Archean IF literature data (3.8–2.6 Ga; 2, 5, 16–2216–22) and modern hydrothermal sediments (23).

Table 1. Estimations of dissolved phosphorus for Carajás based on K_D values taken from adsorption experiments with seawater.

Experimental conditions	K_D values	P (μM)[a]
Seawater + 0 mM Si	0.338	0.004
Seawater + 0.67 mM Si	0.042	0.03
Seawater + 2.2 mM Si	0.008	0.18

[a]Estimated dissolved P based on P/Fe mol ratio (0.0015) for Carajás IFs.

the water column, allowing Fe(II) phosphate mineral (e.g. vivianite) to precipitate (26). Vivianite, once precipitated, can react with calcite with increasing temperature and pressure to form apatite (3). Considering that a reduction of Fe(III) minerals was likely occurring in the Archean (e.g. dissimilatory iron reduction) (16, 27, 28) and that each location was exposed to different metamorphic regimes (e.g. low-greenschist to high-amphibolite facies), it is likely that varying proportions of Fe and P loss will be imprinted in Archean samples, thus supporting the scattering observed in Fig. 2.

In contrast, the preserved correlation between Fe and P in Neoarchean Carajás samples can be explained by two scenarios. These are (i) minimal loss of Fe and P, suggesting remarkable sample preservation, resembling modern hydrothermal environments and/or (ii) loss of Fe and P in similar molar proportions, which would not have affected the primary correlation. The first scenario might have been favored for the Carajás IF considering that it shows abundant carbonate-facies IF, and that the same enhanced alkalinity favoring calcium carbonate precipitation may also act to trap P in sediments by promoting carbonate fluorapatite formation (17). Although the second scenario seems unlikely, we cannot completely exclude it. In any case, this is not critical to our interpretation as it would imply an unmodified P/Fe ratio. Moreover, measured P/Fe ratios from Neoarchean Carajás and Archean literature data both define a log normal distribution (Fig. S5), while P and Fe concentrations show linear correlations with slopes of 0.0013 ($R^2 = 0.97$) for Carajás and 0.0020 ($R^2 = 0.34$) for Archean data (Fig. 2). The P/Fe ratio of Carajás IF is thus not significantly different from that of Archean IFs and it seems reasonable to consider

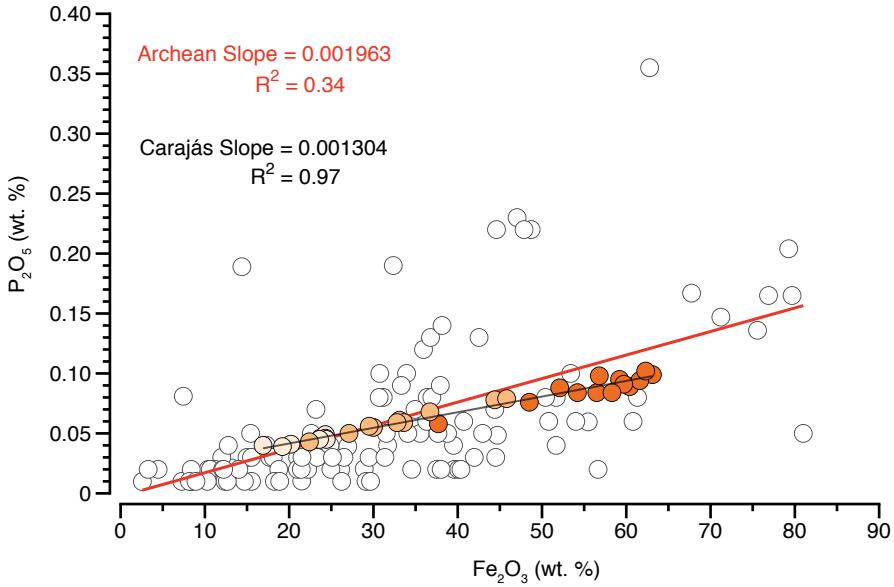

Fig. 2. Comparison of linear regressions based on Fe_2O_3 (wt. %) and P_2O_5 (wt. %) contents from Archean and Carajás data sets showing their respective slopes and R^2 coefficients.

Carajás as a representative but best preserved. Therefore, estimates of dissolved P based on P/Fe ratios in the Archean (e.g. 5, 7) should be well-represented by combining and comparing the two data sets.

Phosphorous-limited Archean ocean

Laboratory experiments have demonstrated that Si and other ferrihydrite-reactive ions may significantly influence P adsorption by competitive interactions, especially Si (10). Given that Archean oceans had a different chemistry compared with modern oceans, Jones et al. (7) proposed a wide range of distribution coefficients (K_D) representative of Precambrian's seawater composition. When combining all K_D values for solutions with varying Si, Ca^{2+}, and Mg^{2+} contents with the P/Fe ratio (0.0015) from the Neoarchean Carajás succession, the estimated dissolved P concentration in paleoseawater ranges from 0.004 μM (for seawater with no dissolved silica) to 0.18 μM (for seawater with 2.2 mM Si) (Table 1). The estimated concentration of 0.004 μM [P] can be regarded as a minimum but unrealistic value, given that Archean seawater was likely Si-rich (10). Concentrations reaching 0.18 μM [P] were calculated based on seawater saturated in Si with respect to amorphous silica (2.2 mM Si). However, Si content reaching 2.2 mM in seawater has been argued as a theoretical maximum for the Precambrian ocean (7). Therefore, dissolved P in Archean seawater during Carajás deposition was likely in the range of $0.004\ \mu M < P_{Carajás}\ \mu M < 0.18\ \mu M$. The highest possible scenario for dissolved P in Carajás paleoseawater (0.18 μM), even though an overestimation, represents only 7.8% of the present-day value. This indicates a low-P content in Carajás paleoseawater compared with that in the modern ocean. It is important to note that these comparisons, as in the case of most prior works treating the Precambrian P cycle, refer to the deep ocean P reservoir that is representative of most of the global oceans in volumetric terms and is also the most likely reservoir recorded by deep-water sediments such as IF. Our estimates are in good agreement with studies advocating low P conditions during the Archean (0.04 to 0.13 μM; 7), but contrast with those arguing for P concentrations similar to (~2.0 μM; 5) or significantly higher than (up to 100 μM; 8, 9) modern values.

In order to discuss the evolution of the marine P reservoir throughout the Archean, it is necessary to establish an approximate value of dissolved Si in ancient seawater. Based on Jones et al. (7), Si concentrations in the Archean ocean were likely between 0.5 and 1.5 mM as determined from Si:Fe ratios in IFs and Si sorption experiments to Fe-oxides. Therefore, here we used a K_D value reflecting seawater with 0.67 mM Si ($K_D = 0.042$), which is the proposed distribution coefficient for Archean seawater in equilibrium with respect to cristobalite, the intermediate scenario between low (0 mM) and high (2.2 mM) Si end members (Jones et al., 2015). Based on this K_D value, we estimated dissolved P using previously measured P/Fe ratios from Archean IFs (18–22, 29, 30), including previously published P compilation data sets (2, 5). We limit our discussion to Archean seawater for which marine P concentrations are highly debated and for which our new data provide important new insights, and refer the reader to other published works for an overview of sedimentary P enrichments over geological time (5, 6).

Based on the varying P/Fe ratios and a K_D value representative of Archean seawater, it is possible to infer that from 3.8 to 2.6 Ga, dissolved P concentrations were on average 0.063 ± 0.05 μM (n = 145), with minimum and maximum values of 0.01 and 0.3 μM, respectively (Fig. 3). Planavsky et al. (5) argued that Archean P levels were similar to modern-day values. However, when applying the same K_D value used in this study to their measured Archean P/Fe ratios (2.95–2.6 Ga), we estimate concentrations of dissolved P to be generally <0.2 μM, thus still supporting low-phosphorus contents in Archean seawater. We were not, however, able to reproduce higher P concentrations from 10 to 100 μM using available IF P/Fe ratio data.

Overestimations of marine P concentrations up to 100 μM during the Archean (8) seem unreasonable in light of the present results. Rasmussen et al. (8) argued that Fe-oxides did not control phosphorus removal from the water column due to the lack of correlation between P and Fe in their Paleoproterozoic data set. However, the authors did not consider that some of these correlations might not be preserved due to later diagenetic effects, such

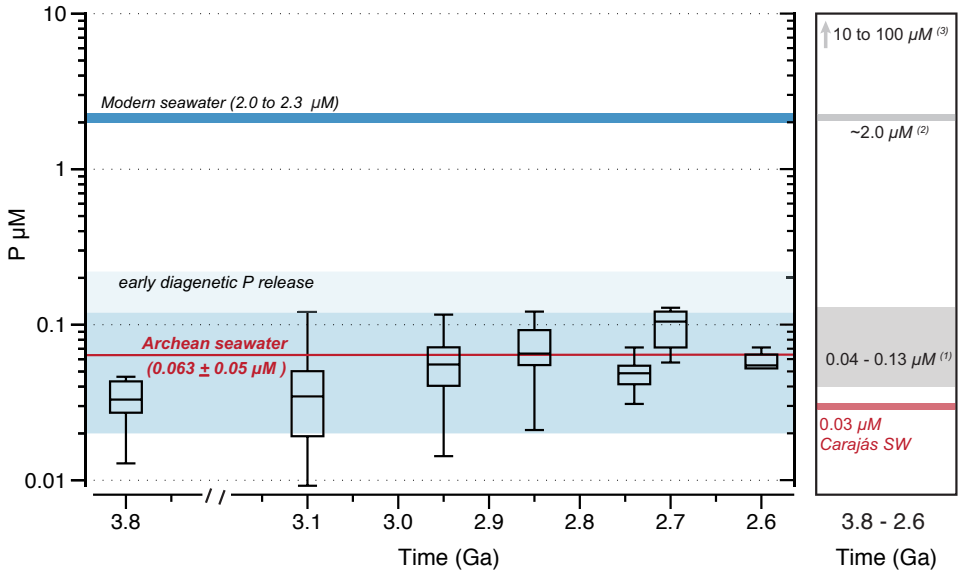

Fig. 3. Box plot showing data distribution for estimates of dissolved phosphorus in Archean seawater with 0.67 mM of Si from 3.8 to 2.6 Ga from measured and literature P/Fe ratios (2, 16–2216–22). Average dissolved P concentration for Archean is shown, while one standard deviation is illustrated by the shaded area. Modern seawater is shown for comparison (11). The right panel summarizes the previous estimates of P concentrations in the Archean ocean (e.g. (1) Jones et al. (7); (2) Planavsky et al. (5); (3) Rasmussen et al. (8)). The range of P concentration of Archean seawater increases when assuming that the sediments experienced a 50% loss during early diagenesis.

as Fe and/or P loss and/or apatite precipitation due to the reaction of vivianite and calcite associated with burial diagenesis (3). Furthermore, it may prove that special conditions (such as high alkalinity favoring P retention via apatite formation) might be required to limit postdepositional P loss and permit the preservation of adsorptive P-Fe scaling relationships in the rock record. Lastly, the authors considered the results obtained on cherts, containing virtually no Fe oxides, to be readily extrapolated to IFs (with 10 to 50 wt.% Fe), which is clearly not the case. The present data set, encompassing a large number of Archean IFs of different ages (16–22), suggests that scavenging of phosphorus by Fe-oxyhydroxide particles was the rule in Archean oceans. This further supports the convention that Fe-oxyhydroxides were indeed a primary mineral phase precipitating from Archean seawater (24). In contrast, the rare evidence available that suggests that Archean seawater P concentrations could have been relatively high (e.g. sustaining calcium phosphate mineral precipitation from seawater; 8) may possibly reflect diagenetic processes or local exceptions.

Our observation of P-Fe scaling relationships in IF consistent with partitioning via a distribution coefficient model provides new support for their application as a proxy of Archean seawater P concentrations, and our new analyses clearly indicate that Earth's ocean surface was likely P-limited. Although the present data (Fig. 1b) suggest minor modifications related to diagenesis, assuming a typical release up to 50% of the adsorbed phosphorus to the overlying seawater (7) would imply that Archean P concentrations were at least 10× lower than modern-day values (Fig. 3). This low P availability likely reflects the balance of more important phosphorous sinks (e.g. IF scavenging) relative to limited sources, such as weathering of emerged continental landmasses, which increased significantly only toward the end of the Archean (4).

Conclusion

Our results provide evidence that scavenging of dissolved P by Fe-oxide precipitates was an active mechanism throughout the Archean Era. The concept of an Fe-P trap mechanism in the Precambrian was first suggested based on modern observational data (2, 11–13), which was later supported by numerical simulations (6, 31). However, clear empirical constraints from the rock record on marine P concentrations in deep time were lacking. IFs from Carajás, combined with a larger Archean literature data set, support the notion of a low-phosphorus ocean and highlight the capability of IFs to record past environmental conditions by the predictable nature of their trace element adsorption reactions. Using the analogous nature of P-Fe partitioning in Carajás IFs compared with modern marine environments as well as experimental studies, we estimated dissolved phosphorus contents in paleoseawater locally and globally, based on measured, experimental, and literature data. We confirm that from 3.8 to 2.6 Ga, phosphorus was most likely scarce in seawater and estimate average concentrations of 0.063 ± 0.05 µM P for this period.

This finding has implications for the P cycle in the Archean and allows us to question whether IF deposition was limiting marine phosphorus concentration. If we take the Carajás basin as an example, we can calculate the flux of P (mol yr^{-1}) exiting seawater based on the average P concentration in IFs, a range of well-constrained sedimentation rates determined for IF (32, 33), and the areal extent of the basin. Considering sedimentation rates of 300, 100, and 6 m $Myear^{-1}$, we determine a high (1.85×10^8 mol $year^{-1}$), medium (6.18×10^7 mol $year^{-1}$), and low (3.71×10^6 mol $year^{-1}$) flux of P for the Carajás basin, respectively. Given the dissolved P concentration (e.g. 0.03 µM) for Carajás paleoseawater, we can thus calculate the P amount in 100 and 1000 m depth and finally estimate a residence time for P in seawater. A maximum residence time of 146 years was calculated for the Carajás basin (i.e. considering 1,000 m depth and low flux of P), which is significantly lower than the residence time of P in the modern ocean (20,000 to 80,000 years; 34). The difference with modern values is even more distinctive if a high flux is considered (e.g. 1.85×10^8 mol $year^{-1}$), providing a residence time of 3 years. Therefore, these results imply that IFs were an important P sink and likely limited P availability in Carajás paleoseawater.

Finally, the long-term availability of phosphorus in Earth's ocean controls the capacity of oxygen to accumulate in the atmosphere by increasing primary biomass production, which will either be buried in sediments, favoring a net O_2 accumulation, or recycled to bioavailable forms (35). Recently, it has been argued that changes in P recycling over time as a result of increased electron acceptors would have modulated biological production (36) and would have been the cause for Earth's major redox tipping point, the GOE (4). Therefore, prior to higher rates of continental weathering and corresponding P influx, and prior to the expansion of sulfidic conditions in continental margins (e.g. less effective P adsorption in sulfides; 37), phosphorous-limited seawater conditions prevailed during the first half of Earth's history and likely contributed strongly to the general anoxia of the atmosphere and ocean throughout much of the Archean Eon.

Materials and methods

For each sample, rock powders representing 10 g or more were crushed in an agate mortar and homogenized, and aliquots of ~250 mg were dissolved in closed teflon vessels (Savillex) at about 90°C for one day using 3 mL of concentrated HF (40%), 3 mL of concentrated HCl (32%), and 1 mL of concentrated HNO_3 (65%). Afterward, 93 mL of H_3BO_3 aqueous solution (20 g L^{-1} H_3BO_3) was added to neutralize the excess HF. All reagents used were of analytical grade. Elements were measured by Inductively Coupled Plasma-Atomic Emission Spectrometry (ICP-AES) using a Horiba Jobin Yvon Ultima 2 spectrometer at the PSO/IUEM (Pôle Spectrométrie Océan, Institut Universitaire Européen de la Mer, Brest, France), following the analytical procedure of Cotten et al. (38). The boron included in the solution was used as an internal standard. The precision and accuracy were evaluated using international standards IF-G, ACE, JB2, and WSE. The relative standard deviation is ≤1% for SiO_2 and ≤2% for the other major elements.

Acknowledgments

This research was funded by Fundação de Amparo à Pesquisa do Estado de São Paulo, FAPESP Projects 2019/16271-0; 2018/05892-0; 2015/16235-2; 2018/02645-2; 2019/16066-7. The authors thank Céline Liorzou for her technical assistance during ICP-AES analyses. V.B. thanks the Institut Universitaire de France for funding (IUF#2017-2021). Parts of this work were supported by the IPGP multidisciplinary program PARI and by Paris-IdF region SESAME, under grant no. 12015908

Supplementary material

Supplementary material is available at *PNAS Nexus* online.

Author contributions

E.S.R.: conceptualization, investigation, visualization, and writing of the original draft. V.B.: conceptualization, investigation, visualization, writing reviews, and editing. S.L.: conceptualization, investigation, writing reviews, and editing. C.R.: investigation, writing reviews, and editing. M.B. provided the resources, writing reviews and editing. P.P.: conceptualization, investigation, funding acquisition, resources, writing reviews, and editing.

Data availability

All data are included in the article and/or supplementary material.

References

1 Tyrrell T. 1999. The relative influences of nitrogen and phosphorus on oceanic primary production. *Nature* 400:525–531.
2 Bjerrum CJ, Canfield DE. 2002. Ocean productivity before about 1.9 Gyr ago limited by phosphorus adsorption onto iron oxides. *Nature* 417:159–162.
3 Hao J, Knoll AH, Huang F, Hazen RM, Daniel I. 2020. Cycling phosphorus on the Archean Earth: part I. Continental weathering and riverine transport of phosphorus. *Geochim Cosmochim Acta*. 273:70–84.
4 Alcott LJ, Mills BJW, Bekker A, Poulton SW. 2022. Earth's great oxidation event facilitated by the rise of sedimentary phosphorus recycling. *Nat Geosci*. 15:210–215.
5 Planavsky NJ, *et al.* 2010. The evolution of the marine phosphate reservoir. *Nature* 467:1088–1090.
6 Reinhard CT, *et al.* 2017. Evolution of the global phosphorus cycle. *Nature* 541:386–389.
7 Jones C, Nomosatryo S, Crowe SA, Bjerrum CJ, Canfield DE. 2015. Iron oxides, divalent cations, silica, and the early earth phosphorus crisis. *Geology* 43:135–138.
8 Rasmussen B, Muhling JR, Suvorova A, Fischer WW. 2021. Apatite nanoparticles in 3.46-2.46 Ga iron formations: evidence for phosphorus-rich hydrothermal plumes on early Earth. *Geology* 49:647–651.
9 Ingalls M, Grotzinger JP, Present T, Rasmussen B, Fischer WW. 2022. Carbonate-associated phosphate (CAP) indicates elevated phosphate availability in Neoarchean shallow marine environments. *Geophys Res Lett*. 49:e2022GL098100.
10 Konhauser KO, Lalonde SV, Amskold L, Holland HD. 2007. Was there really an Archean phosphate crisis? *Science* 315:1234.
11 Feely RA, Trefry JH, Lebon GT, German CR. 1998. The relationship between P/Fe and V/Fe ratios in hydrothermal precipitates and dissolved phosphate in seawater. *Geophys Res Lett*. 25:2253–2256.
12 Berner RA. 1973. Phosphate removal from sea water by adsorption on volcanogenic ferric oxides. *Earth Planet Sci Lett*. 18:77–86.
13 Wheat CG, Feely RA, Mottl MJ. 1996. Phosphate removal by oceanic hydrothermal processes: an update of the phosphorus budget in the oceans. *Geochim Cosmochim Acta*. 60:3593–3608.
14 Herschy B, *et al.* 2018. Archean phosphorus liberation induced by iron redox geochemistry. *Nat Commun*. 9:1–7.
15 Pasek MA, Harnmeijerbc JP, Buickb R, Gulla M, Atlasa Z. 2013. Evidence for reactive reduced phosphorus species in the early Archean ocean. *Proc Natl Acad Sci U S A*. 110:10089–10094.
16 Marin-Carbonne J, *et al.* 2020. In situ Fe and S isotope analyses in pyrite from the 3.2 Ga Mendon Formation (Barberton Greenstone Belt, South Africa): evidence for early microbial iron reduction. *Geobiology* 18:306–325.
17 Zhao M, Zhang S, Tarhan LG, Reinhard CT, Planavsky N. 2020. The role of calcium in regulating marine phosphorus burial and atmospheric oxygenation. *Nat Commun*. 11:2232.
18 Bhattacharya HN, Chakraborty I, Ghosh KK. 2007. Geochemistry of some banded iron-formations of the Archean supracrustals, Jharkhand-Orissa region, India. *J Earth Syst Sci*. 116:245–259.
19 Cates NL, Mojzsis SJ. 2007. Pre-3750 Ma supracrustal rocks from the Nuvvuagittuq supracrustal belt, northern Québec. *Earth Planet Sci Lett*. 255:9–21.
20 Alexander BW, Bau M, Andersson P, Dulski P. 2008. Continentally-derived solutes in shallow Archean seawater:

rare earth element and Nd isotope evidence in iron formation from the 2.9 Ga Pongola Supergroup, South Africa. *Geochim Cosmochim Acta*. 72:378–394.
21 Nutman AP, Friend CRL, Bennett VC, Wright D, Norman MD. 2010. ≥3700ma pre-metamorphic dolomite formed by microbial mediation in the Isua supracrustal belt (W. Greenland): simple evidence for early life? *Precambrian Res*. 183:725–737.
22 Mloszewska AM, *et al.* 2012. The composition of Earth's Oldest iron formations: the Nuvvuagittuq Supracrustal Belt (Québec, Canada). *Earth Planet Sci Lett*. 317–318:331–342.
23 Lyle M. 1986. Major element composition of leg 92 sediments. *Initial Reports Deep Sea Drill Proj*. 92:355–370.
24 Robbins LJ, *et al.* 2019. Hydrogeological constraints on the formation of Palaeoproterozoic banded iron formations. *Nat Geosci*. 12: 558–563.
25 Dauphas N, *et al.* 2007. Iron isotope, major and trace element characterization of early Archean supracrustal rocks from SW Greenland: protolith identification and metamorphic overprint. *Geochim Cosmochim Acta*. 71:4745–4770.
26 Busigny V, *et al.* 2016. The iron wheel in lac pavin: interaction with phosphorus cycle. In: Sime-Ngando T, Boivin P, Chapron E, Jezequel D, Meybeck M, editors. *Lake pavin: history, geology, biogeochemistry, and sedimentology of a deep meromictic maar lake*. India: Springer International Publishing. p. 205–220.
27 Archer C, Vance D. 2006. Coupled Fe and S isotope evidence for Archean microbial Fe(III) and sulfate reduction. *Geology* 34:153–156.
28 Craddock PR, Dauphas N. 2011. Iron and carbon isotope evidence for microbial iron respiration throughout the Archean. *Earth Planet Sci Lett*. 303:121–132.
29 Smith AJB, Beukes NJ, Gutzmer J. 2013. The composition and depositional environments of Mesoarchean iron formations of the West Rand Group of the Witwatersrand Supergroup, South Africa. *Econ Geol*. 108:111–134.
30 Haugaard R, Ootes L, Creaser RA, Konhauser KO. 2016. The nature of Mesoarchaean seawater and continental weathering in 2.85 Ga banded iron formation, Slave Craton, NW Canada. *Geochim Cosmochim Acta*. 194:34–56.
31 Derry LA. 2015. Causes and consequences of mid-Proterozoic anoxia. *Geophys Res Lett*. 42:8538–8546.
32 Konhauser KO, *et al.* 2018. Phytoplankton contributions to the trace-element composition of Precambrian banded iron formations. *Bull Geol Soc Am*. 130:941–951.
33 Lantink ML, Davies JHFL, Mason PRD, Schaltegger U, Hilgen FJ. 2019. Climate control on banded iron formations linked to orbital eccentricity. *Nat Geosci*. 12:369–374.
34 Benitez-Nelson CR. 2000. The biogeochemical cycling of phosphorus in marine systems. *Earth Sci Rev*. 51:109–135.
35 Reinhard CT, Planavsky NJ. 2020. Biogeochemical controls on the redox evolution of earth's oceans and atmosphere. *Elements* 16: 191–196.
36 Kipp MA, Stüeken EE. 2017. Biomass recycling and Earth's early phosphorus cycle. *Sci Adv*. 3:1–7.
37 Kraal P, van Genuchten CM, Behrends T. 2022. Phosphate coprecipitation affects reactivity of iron (oxyhydr)oxides towards dissolved iron and sulfide. *Geochim Cosmochim Acta*. 321:311–328.
38 Cotten J, *et al.* 1995. Origin of anomalous rare-earth element and yttrium enrichments in subaerially exposed basalts: evidence from French Polynesia. *Chem Geol*. 119:115–138.

Supplementary Material: Low phosphorus concentrations and important ferric hydroxide scavenging in Archean seawater

Eric Siciliano Rego[1,2,*]; Vincent Busigny[3]; Stefan V. Lalonde[4]; Camille Rossignol[5]; Marly Babinski[1]; Pascal Philippot[2,6]

GEOLOGICAL CONTEXT

The Carajás Mineral Province (CMP) is located in the southeastern part of the Amazonian Craton, Brazil (Fig. S1 A), and contains remarkable metallogenic diversity including world-class deposits of iron oxide-copper-gold (IOCG), large IFs, and Mn ore (1, 2). The Carajás Basin, within the CMP (Fig. S1 B,C), comprises Neoarchean and Paleoproterozoic sedimentary units that have been deposited on a basement made up of granulites, migmatites and metavolcanic rocks emplaced from ca. 3080 Ma to ca. 3000 Ma (2–4). The crystalline basement is overlain unconformably by volcano-sedimentary sequences from the Grão Pará Group, which have undergone subgreenschist to low-greenschist facies metamorphism (4–6). At the base of the Grão Pará Group lies the Parauapebas Formation, composed by basalts and basaltic andesites, while IFs from the Carajás Formation conformably overlie or are occasionally interlayered with the basalts, a typical characteristic of Algoma-type IFs (1, 7, 8). The main lithologies comprising the Carajás Formation are oxide-facies banded iron formations alternating iron-rich and chert layers, but minor black shales and conglomeratic layers have also been reported (9, 10). These were interpreted to have been deposited in a range of environments from shallow water, low energy environments, to deep and quiet water settings (11–15).

A Late Archean to Early Paleoproterozoic sedimentary cover overlies the IFs, however its age is still debated (16). The depositional age of the Carajás IFs is well-constrained by U-Pb zircon ages of ca. 2.76-2.75 Ga in the basalts underlying and intercalating the IFs (2759 ± 2 Ma, (4); 2751 ± 4, (6)) and U-Pb zircon ages from a possible tuff (2743 ± 11 Ma) and a dolerite dyke (2740 ± 8 Ma) cross-cutting the Carajás Formation (18). The iron deposits have an average thickness of 200-250 m in the Serra Norte and 300 m in the Serra Sul regions (19). The drill core FD-55 intercepting the IF deposit in Serra Norte was selected for this study (Fig. S1 D), particularly because it has two carbonate-rich intervals intercalated with iron formations, thus reflecting changes in depositional environments (*e.g.* shallower and deeper settings).

The IF facies in core FD-55 is characterized by alternating layers of Fe-rich minerals (magnetite and hematite) and chert with microcrystalline quartz and a few Fe-carbonate (*e.g.* ankerite) disseminated in the matrix. Laminations are mm- to cm-thick and usually exhibit an homogeneous banding (Fig. S2 A). Some laminations however display wavy structures (Fig. S2 B), pinching geometries and erosion surfaces (Fig. S2 C). A gradual change is observed from IF facies to Fe-rich/IF carbonates and Fe-poor carbonates (20). The Fe-rich carbonates also comprise banded (Fig. S3 A), wavy (Fig. S3 B) and irregular Fe-oxides (mainly magnetite) layers (Fig. S3 C), while carbonate phases consist mainly of ankerite with minor calcite. Iron-poor carbonate facies show mm- to cm-thick wavy to crinkly carbonates laminae and minor iron oxides (Fig. S3 D,E). As carbonate content increases (calcite and ankerite), distinct intervals containing framboidal pyrites and organic matter were also identified (Fig. S2F, G).

Supplementary Figure and Tables:

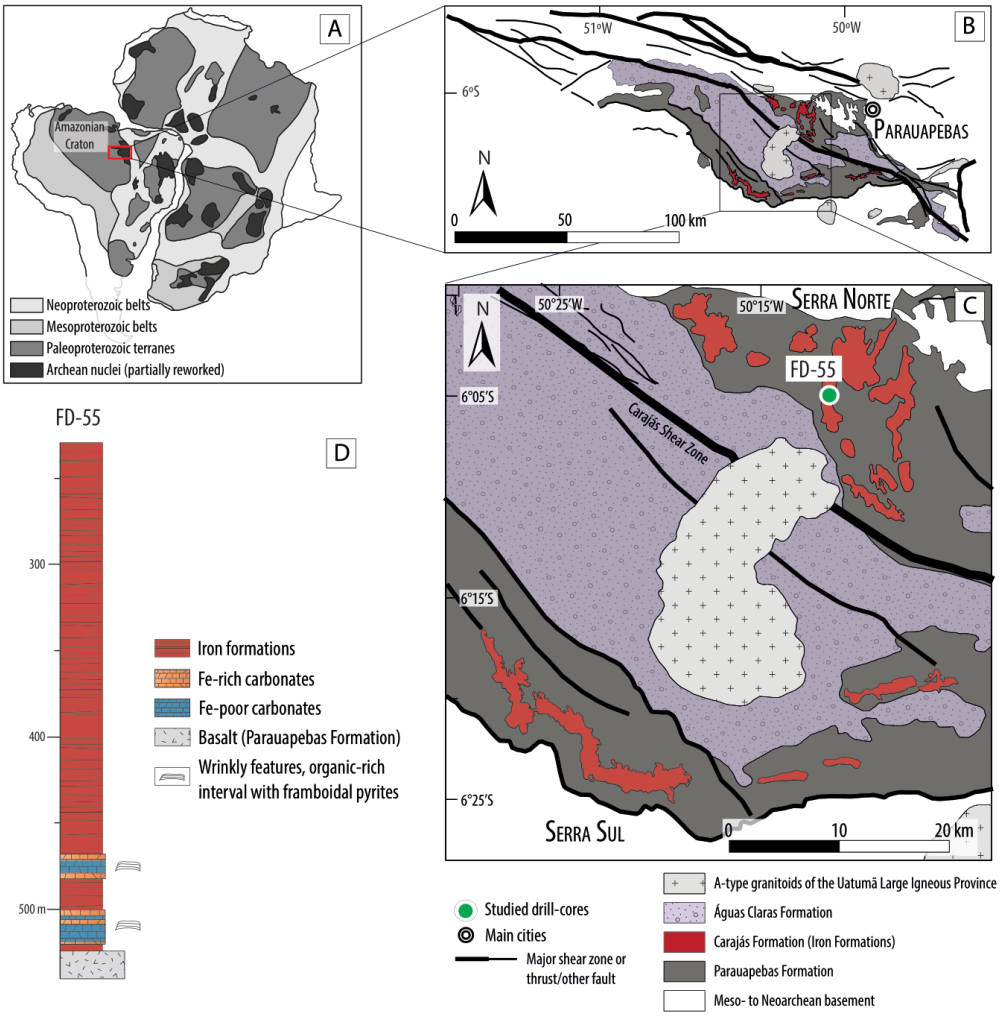

Fig. S1 Geological map of the Carajás basin, located in the southeastern portion of the Amazonian Craton (A), showing the location of the drill core FD-55 in Serra Norte (B,C) and the main lithological components varying as a function of depth (m) (D) (after Rego et al., 2021).

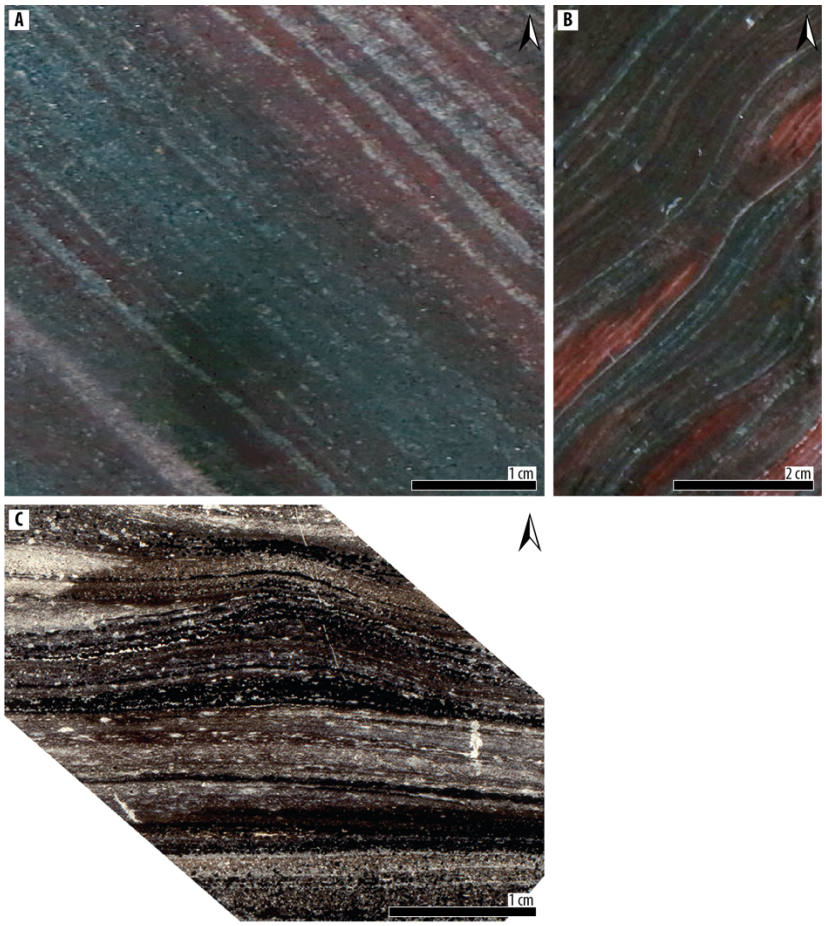

Fig. S2. Banded iron facies from the Carajás Formation. Arrows point to the stratigraphic top. **A**. Sample FD55-486.45. Fine horizontal laminations (sub-mm scale) of iron-bearing minerals (magnetite and hematite) and chert layers. **B**. Sample FD55-495.80. Finely laminated siliceous BIF displaying wavy laminations. **C.** Sample FD55-480.80. Thin section in reflected light showing a reactivation surface in a jaspilitic BIF.

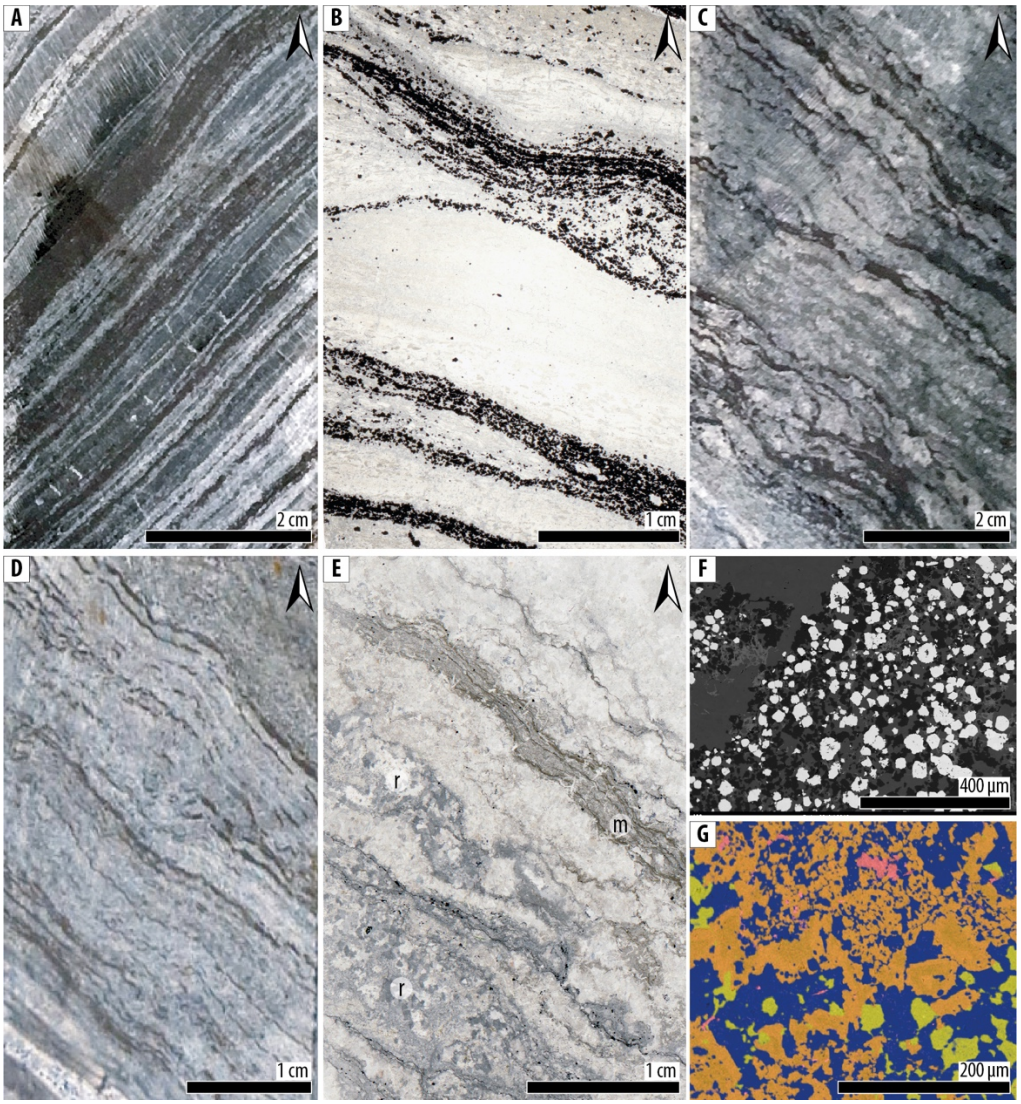

Fig. S3. Carbonate facies of the Carajás Formation. Arrows point to the stratigraphic top. **A.** Sample FD55-521.60. Fine laminations (mm to cm scale) of iron-bearing minerals (mainly magnetite) and carbonate layers. **B.** Sample FD55-521.12. Thin section in reflected light showing wavy laminations underlined by magnetite grains and carbonates. **C.** Sample FD55-518.50. Carbonate with irregular, crinkled magnetite laminations and pinching out geometries. **D.** Sample FD55-522.56. Carbonate with very fine, crinkled lamination underlined by very fine (mm thick) magnetite layers. **E.** Sample FD55-520.06. Thin section in reflected light showing a microbial mat (m) within carbonate displaying a clotted micritic texture. Some areas show recrystallized (r) textures. **F.** Sample FD55-514.57. Electron backscattered image showing diagenetic framboidal pyrite (bright white) minerals within a carbonate matrix. **G.** Sample FD55-514.57. EDS electron image showing Si, Ca and Fe-rich mineral phases.

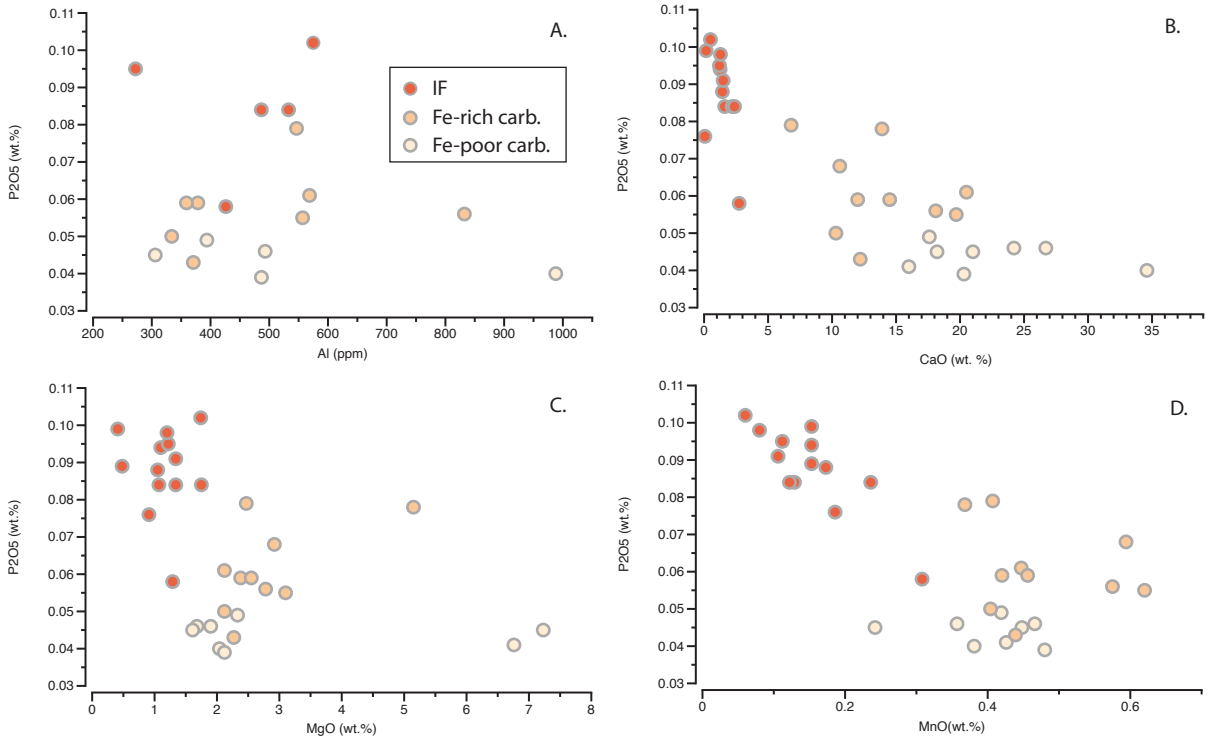

73

74 **Fig. S4**: Variations in bulk P_2O_5, Al, CaO, MgO, and MnO measured in Neoarchean iron

75 formations, Fe-rich and Fe-poor carbonates from Carajás, Brazil.

76

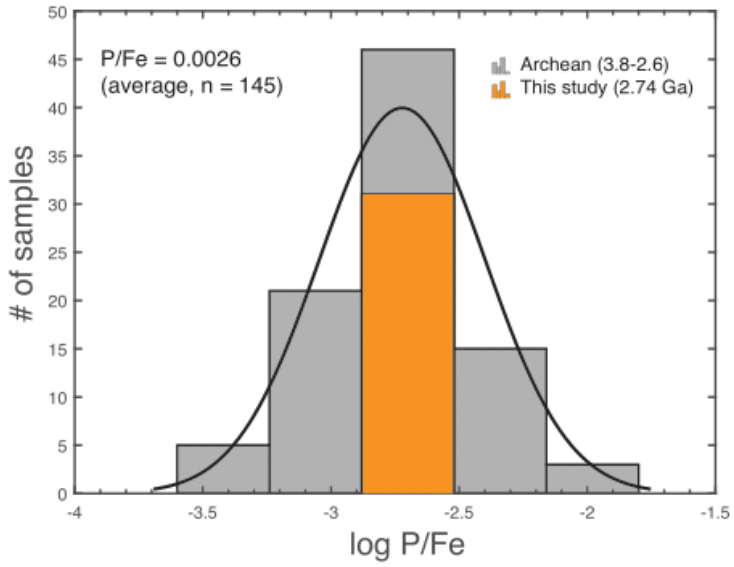

Fig. S5. Normal distribution shown by log P/Fe ratios from Archean and Neoarchean Carajás (this study) IFs fitted with a gaussian distribution curve.

Table S2: Estimations of dissolved P for Carajás samples based on K_D values taken from NaCl and seawater experiments, including additional K_D values based of experimental condition reproducing an ancient ocean with varying Si, Ca^{2+}, and Mg^{2+} contents (Konhauser et al., 2007; Jones et al., 2015).

Experimental Conditions	K_D values	P (μM)[1]
(Konhauser et al., 2007)		
NaCl + 0 Si	0.075	0.02
NaCl + 0.67 mM Si	0.011	0.13
NaCl + 2.2 mM Si	0.002	0.73
(Jones et al., 2015)		
Seawater + 0 mM Si	0.338	0.004
Seawater + 0.67 mM Si	0.042	0.03
Seawater + 2.2 mM Si	0.008	0.18
0.56 M NaCl + 0 mM Si	0.078	0.02
0.56 M NaCl + 0.67 mM Si	0.01	0.15
0.56 M NaCl + 0.67 mM Si + 50 mM Mg2+	0.054	0.03
0.56 M NaCl + 0.67 mM Si + 10 mM Ca2+	0.119	0.01
0.56 M NaCl + 0.67 mM Si + 50 mM Mg2+ + 10 mM Ca2+ (modern ocean [Ca and Mg])	0.066	0.02
0.56 M NaCl + 2.2 mM Si + 45 mM Mg2+ + 55 mM Ca2+ (ancient calcite sea)	0.021	0.07
0.56 M NaCl + 2.2 mM Si + 10 mM Mg2+ + 24 mM Ca2+ (ancient aragonite sea)	0.013	0.11
0.56 M NaCl + 0 mM Si + 50 mM Mg2+ + 10 mM Ca2+	0.23	0.006

[1]Estimated dissolved P based on P/Fe mol ratio (0.0015) for Carajás IFs (2.74 Ga).

REFERENCES CITED

1. C. Klein, E. A. Ladeira, Petrography and geochemistry of the least altered banded iron-formation of the Archean Carajás formation, northern Brazil. *Econ. Geol.* **97**, 643–651 (2002).
2. C. P. N. Moreto, *et al.*, Neoarchean and paleoproterozoic iron oxide-copper-gold events at the sossego deposit, Carajás Province, Brazil: Re-Os and U-Pb geochronological evidence. *Econ. Geol.* **110**, 809–835 (2015).
3. R. T. Pidgeon, M. J. B. MacAmbira, J. M. Lafon, Th-U-Pb isotopic systems and internal structures of complex zircons from an enderbite from the Pium Complex, Carajas Province, Brazil: Evidence for the ages of granulite facies metamorphism and the protolith of the enderbite. *Chem. Geol.* **166**, 159–171 (2000).
4. N. Machado, Z. Lindenmayer, T. E. Krogh, D. Lindenmayer, U-Pb geochronology of Archean magmatism and basement reactivation in the Carajás area, Amazon shield, Brazil. *Precambrian Res.* **49**, 329–354 (1991).
5. C. A. Rosière, *et al.*, Structure and iron mineralisation of the Carajás Province. *Trans. Institutions Min. Metall. Sect. B Appl. Earth Sci.* **115**, 126–133 (2006).
6. R. S. Krymsky, M. J. B. Macambira, J. M. Lafon, G. S. Estumano, Uranium-lead dating method at the Pará-Iso isotope geology laboratory, UFPA, Belém - Brazil. *An. Acad. Bras. Cienc.* **79**, 115–128 (2007).
7. P. L. G. Martins, *et al.*, Neoarchean magmatism in the southeastern Amazonian Craton, Brazil: Petrography, geochemistry and tectonic significance of basalts from the Carajás Basin. *Precambrian Res.* **302**, 340–357 (2017).
8. H. Dalstra, S. Guedes, Giant hydrothermal hematite deposits with Mg-Fe metasomatism:

A comparison of the Carajás, Hamersley, and other iron ores. *Econ. Geol.* **99**, 1793–1800 (2004).

9. A. R. Cabral, *et al.*, Trace-element and multi-isotope geochemistry of Late-Archean black shales in the Carajás iron-ore district, Brazil. *Chem. Geol.* **362**, 91–104 (2013).

10. A. R. Cabral, *et al.*, Multiple sulfur isotopes from the Neoarchaean Serra Sul black shale, Carajás mineral province, northern Brazil. *J. South Am. Earth Sci.* **79**, 377–383 (2017).

11. G. E. Tolbert, J. W. Tremaine, G. C. Melcher, C. B. Gomes, The Recently Discovered Serra dos Carajas Iron Deposits, Northern Brazil. *Econ. Geol.* **66**, 985–994 (1971).

12. J. B. Macambira, A. Schrank, Químio-estratigrafia e evolução dos jaspilitos da Formação Carajás (PA). *Rev. Bras. Geociências* **32**, 567–578 (2002).

13. B. Ribeiro da Luz, J. K. Crowley, Morphological and chemical evidence of stromatolitic deposits in the 2.75Ga Carajás banded iron formation, Brazil. *Earth Planet. Sci. Lett.* **355**–**356**, 60–72 (2012).

14. Z. Lindenmayer, J. Laux, J. Teixeira, Consideração sobre a origem das formações ferríferas da Formação Carajás, Serra dos Carajás. *Rev. Bras. Geociências* **31**, 21–28 (2001).

15. A. P. Justo, *et al.*, Paleobasinal to band-scale REE + Y distribution in iron formations from Carajás, Amazon Craton, Brazil. *Ore Geol. Rev.* **127**, 103750 (2020).

16. C. Rossignol, *et al.*, Stratigraphy and geochronological constraints of the Serra Sul Formation (Carajás Basin, Amazonian Craton, Brazil). *Precambrian Res.* **351**, 105981 (2020).

17. A. K. Gibbs, K. R. Wirth, W. K. Hirata, W. J. Olszewski, Age and composition of the Grão Pará Group volcanics, Serra dos Carajás. *Rev. Bras. Geociências* **16**, 201–211

(1986).

18. A. F. Trendall, M. A. S. Basei, J. R. De Laeter, D. R. Nelson, SHRIMP zircon U-Pb constraints on the age of the Carajas formation, Grao Para Group, Amazon Craton. *J. South Am. Earth Sci.* **11**, 265–277 (1998).

19. V. D. R. Beisiegel, A. L. Bernardelli, N. F. Drummond, A. W. Ruff, J. W. R. Tremaine, Geologia e Recursos Minerais da Serra dos Carajás. *Rev. Bras. Geociências* **3**, 215–242 (1973).

20. E. S. Rego, *et al.*, Anoxygenic photosynthesis linked to Neoarchean iron formations in Carajás (Brazil). *Geobiology* **19**, 326–341 (2021).

Table S1: Major element concentrations measured in Carajás samples, including Iron Formations, Fe-rich and Fe-poor carbonate.

Sample depth	Lithology	Al (ppm)*	SiO2 %	TiO2 %	Fe2O3 %	MnO %	MgO %	CaO %	Na2O %	K2O %	P2O5 %	LOI
FD55 280.90_96	IFs	< D.L.	34,7	0,01	63,1	0,153	0,41	0,16	<LD	<LD	0,099	0,76
FD55 295.75_85	IFs	< D.L.	36,6	0,01	60,4	0,153	0,48	NaN	<LD	0,00	0,089	0,51
FD55 311.75_80	IFs	< D.L.	50,3	0,01	48,5	0,186	0,91	0,06	<LD	<LD	0,076	0,68
FD55 331.04_09	IFs	< D.L.	35,4	0,01	61,6	0,153	1,10	1,25	<LD	0,00	0,094	0,98
FD55 356.76_78	IFs	426,08	54,2	0,01	37,7	0,308	1,29	2,74	<LD	<LD	0,058	3,33
FD55 369.96_370.02	IFs	< D.L.	38,4	0,01	56,5	0,236	1,07	1,61	<LD	0,00	0,084	0,97
FD55 384.40_46	IFs	< D.L.	43,6	0,01	52,1	0,173	1,05	1,43	<LD	0,00	0,088	0,98
FD55 399.70_77	IFs	574,95	33,3	0,01	62,3	0,060	1,74	0,50	<LD	<LD	0,102	-0,47
FD55 414.17_22	IFs	272,29	37,6	0,01	59,2	0,112	1,22	1,20	<LD	<LD	0,095	1,16
FD55 426.07_15	IFs	< D.L.	40,8	0,01	56,8	0,080	1,20	1,28	<LD	<LD	0,098	0,59
FD55 438.93_99	IFs	< D.L.	35,7	0,01	59,7	0,106	1,34	1,49	<LD	<LD	0,091	0,90
FD55 478.03_13	Fe-poor carbonate	< D.L.	24,6	0,01	23,7	0,357	1,68	26,7	0,00	0,00	0,046	24,23
FD55 478.34_42	Fe-poor carbonate	393,79	34,7	0,01	24,3	0,419	2,33	17,6	0,00	0,00	0,049	20,46
FD55 478.98_479.02	Fe-rich carbonate	568,67	19,0	0,01	33,1	0,447	2,12	20,5	0,00	0,00	0,061	23,59
FD55 479.05_10	Fe-poor carbonate	493,09	21,3	0,01	24,3	0,466	1,90	24,21	0,00	<LD	0,046	26,96
FD55 495.87_90	IFs	532,91	39,8	0,01	54,2	0,129	1,34	2,20	<LD	<LD	0,084	2,41
FD55 503.22_30	IFs	486,55	34,1	0,01	58,3	0,122	1,75	2,38	<LD	<LD	0,084	2,42
FD55 511.92_512.03	Fe-poor carbonate	< D.L.	34,3	0,01	24,4	0,242	1,61	21,0	0,00	0,00	0,045	18,81
FD55 512.59_65	Fe-rich carbonate	5427,94	15,3	0,01	44,4	0,368	5,15	13,9	0,08	0,27	0,078	18,52
FD55 512.98_513.06	Fe-poor carbonate	< D.L.	35,7	0,01	20,2	0,426	6,76	16,0	0,00	0,00	0,041	22,50
FD55 513.72_80	Fe-poor carbonate	305,90	25,0	0,01	23,6	0,448	7,23	18,2	0,00	0,00	0,045	25,89
FD55 515.23_30	Fe-poor carbonate	987,93	14,7	0,01	16,9	0,381	2,04	34,6	0,00	0,02	0,040	29,70
FD55 515.34_41	Fe-rich carbonate	556,81	23,2	0,01	30,0	0,620	3,10	19,7	0,00	0,00	0,055	22,73
FD55 517.15_25	Fe-rich carbonate	378,38	35,0	0,01	33,6	0,420	2,38	12,0	0,00	0,00	0,059	15,46
FD55 517.65_70	Fe-poor carbonate	486,69	36,3	0,01	19,2	0,480	2,12	20,3	0,00	0,01	0,039	22,28
FD55 517.70_78	Fe-rich carbonate	832,34	24,9	0,01	29,5	0,575	2,78	18,1	0,00	0,01	0,056	22,32
FD55 518.53_60	Fe-rich carbonate	358,99	30,2	0,01	32,8	0,456	2,55	14,5	0,00	0,00	0,059	18,10
FD55 520.38_48	Fe-rich carbonate	< D.L.	29,3	0,01	36,7	0,594	2,92	10,6	0,00	0,00	0,068	17,97
FD55 520.58_66	Fe-rich carbonate	370,68	46,8	0,01	22,4	0,439	2,27	12,2	0,00	0,00	0,043	15,85
FD55 520.66_73	Fe-rich carbonate	333,96	47,0	0,01	27,1	0,404	2,12	10,3	0,00	0,00	0,050	13,62
FD55 521.63_73	Fe-rich carbonate	546,50	35,3	0,01	45,8	0,407	2,47	6,8	0,00	0,00	0,079	9,09

*from Rego et al., 2021